Markus Hautakorpi and Matti Kaivola. 2006. Modal analysis of the self-imaging phenomenon in optical fibers with an annular core. Applied Optics, volume 45, number 25, pages 6388-6392.

Modal analysis of the self-imaging phenomenon in optical fibers with an annular core

Markus Hautakorpi and Matti Kaivola

We investigate the occurrence of self-images, or Talbot images, in a spatially multimode field that propagates along an optical fiber whose core has an annular-shaped cross section. By use of full-vectorial modal analysis, we study the effect of the transverse fiber dimensions on the self-imaging properties. According to our analysis, good self-images can be expected when the fiber core is thin and the modes are far from their cutoffs. However, as the core diameter is made larger to increase the number of modes available in the imaging, the general self-imaging properties tend to deteriorate.

OCIS codes: 060.2310, 060.2340, 060.2350, 260.2110.

1. Introduction

Within the scalar diffraction theory, a laterally periodic optical field will produce exact replicas of itself upon propagation, thus possessing spatial periodicity also in the propagation direction.[1] This kind of self-imaging phenomenon is known as the Talbot effect for historical reasons, and it occurs naturally with optical systems that are periodic in Cartesian coordinates, such as with linear diffraction gratings, and approximately also with periodic fields in dielectric slab waveguides. An approximate self-imaging effect can be encountered as well with cylindrical multimode waveguides,[2,3] and, in particular, with optical fibers having annular-shaped cores.[4–6] It has been demonstrated that such annular dielectric waveguides can be fabricated with a femtosecond-pulse laser-writing technique,[7] and that their self-imaging ability can be applied in phase locking of a circular array of fiber lasers.[8,9]

Theoretical studies dealing with the self-imaging phenomenon in annular-core fibers have, so far, been restricted to the domain of scalar optics by means of the weakly guiding approximation.[5,6,8] In such annular fibers, however, the approximation may not be very accurate, especially if the fiber core is very thin, and it has a large diameter.[10] On the other hand, it is often argued that fibers with exactly these characteristics should be chosen for the self-imaging applications.[4,5,8] We apply full-vectorial modal analysis to both small- and large-diameter fibers to determine the effect of the transverse core dimensions on self-imaging properties. In addition to improved accuracy over the weakly guiding approximation, we also take into account the beating effect associated with the propagation of vector modes with only slightly different propagation constants.

In Section 2 we briefly describe the method of obtaining the propagation constants and the modal profiles of the electromagnetic vector modes in an annular-core fiber. Then by arranging the propagation constants appropriately, we describe the Talbot effect with a model similar to that often used with the weakly guiding approximation. The discrepancies from this model are characterized in terms of the standard deviation of modal phases at the Talbot image plane. In Section 3 we present the results of the numerical analysis performed for fibers with different transverse sizes, and finally in Section 4, we draw conclusions from the obtained results.

2. Properties of the Vector Modes and the Model for Self-Imaging

The propagating vector modes of an annular-core fiber are found by solving Helmholtz's wave equation,[11]

$$\left(\nabla^2 + k^2 n_j^2\right)\begin{Bmatrix}\mathbf{E}(\mathbf{r})\\ \mathbf{H}(\mathbf{r})\end{Bmatrix} = 0, \tag{1}$$

The authors are with Optics and Molecular Materials, Helsinki University of Technology, P. O. Box 3500, FI-02015 HUT, Finland. M. Hautakorpi's e-mail address is Markus.Hautakorpi@tkk.fi.

Received 1 December 2005; revised 8 June 2006; accepted 15 June 2006; posted 15 June 2006 (Doc. ID 66349).

0003-6935/06/256388-05$15.00/0

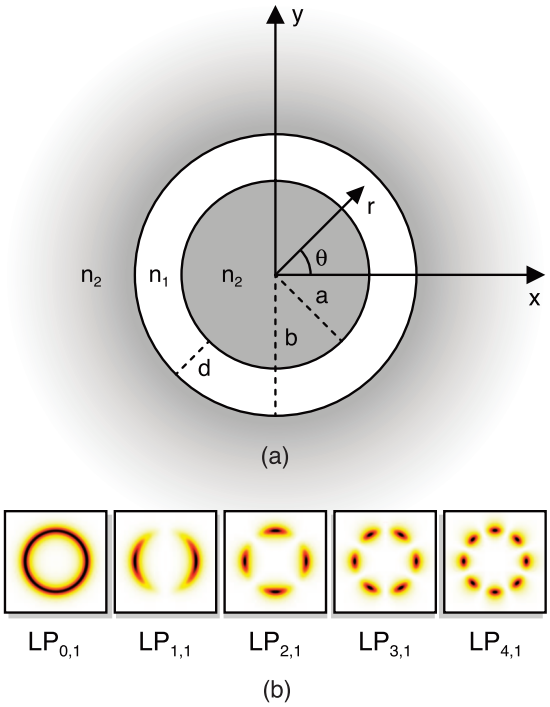

Fig. 1. (Color online) (a) Cross section of an annular-core optical fiber with inner and outer core radii denoted by a and b, respectively, and with a core thickness of $d = b - a$. The refractive-index n_1 of the core is slightly higher than that of the inner and outer claddings, n_2. (b) Transverse intensity patterns of the $LP_{m,p}$ modes of a fiber with $a = 15\lambda$, $d = 3\lambda$, $n_1 = 1.457$, and $n_2 = 1.455$, with λ denoting the vacuum wavelength.

where the upper and lower rows stand for the spatial parts of the electric and magnetic fields, $\mathbf{E}(\mathbf{r})$ and $\mathbf{H}(\mathbf{r})$, respectively, with $\mathbf{r} = (r, \theta, z)$ denoting a point in cylindrical coordinates. The wavenumber is denoted with $k = \omega/c$, where ω and c are the angular frequency and the speed of light in vacuum, respectively, and n_j is used to denote the refractive indices of the core ($j = 1$) and the cladding ($j = 2$) [see Fig. 1(a)]. The full time-dependent electric and magnetic fields of a mode propagating to the positive z direction are of the form $\mathbf{E}(\mathbf{r}; t) = \mathbf{E}(r, \theta)\exp[i(\omega t - \beta z)]$ and $\mathbf{H}(\mathbf{r}; t) = \mathbf{H}(r, \theta)\exp[i(\omega t - \beta z)]$, respectively, where t denotes time and β is the propagation constant. To solve the electromagnetic field of a mode, one usually first specifies the longitudinal field components E_z and H_z, which are then used to derive the transverse components with the help of Maxwell's curl equations. In our annular waveguide, the trial function for the longitudinal electric field component is written as[10]

$$E_z(r, \theta) = \begin{cases} C_1 I_l(vr)\sin(l\theta + \phi), & r \le a, \\ [C_2 J_l(ur) + C_3 N_l(ur)]\sin(l\theta + \phi), & a < r < b, \\ C_4 K_l(vr)\sin(l\theta + \phi), & b \le r, \end{cases} \quad (2)$$

with a similar expression for the magnetic field:

$$H_z(r, \theta) = \begin{cases} C_5 I_l(vr)\cos(l\theta + \phi), & r \le a, \\ [C_6 J_l(ur) + C_7 N_l(ur)]\cos(l\theta + \phi), & a < r < b, \\ C_8 K_l(vr)\cos(l\theta + \phi), & b \le r. \end{cases} \quad (3)$$

In Eqs. (2) and (3), J_l and N_l (I_l and K_l) denote the (modified) Bessel functions of the first and second kinds of order l, respectively. Furthermore, the parameters u and v are given by $u = (k^2 n_1^2 - \beta^2)^{1/2}$ and $v = (\beta^2 - k^2 n_2^2)^{1/2}$, and the parameter ϕ is an arbitrary phase angle. Propagation constant β and constants $C_1, \ldots, C_8$ are determined for each mode by requiring that the tangential components E_z, E_θ, H_z, and H_θ should be continuous over the core boundaries at $r = a$ and $r = b$. Such boundary conditions yield a set of eight homogeneous equations, from which the allowed values of β and constants $C_1, \ldots, C_8$ can be obtained. We note that the formulation described above for finding the modes is a straightforward generalization of the modal theory of standard step-index fibers,[12,13] when adjusted to the annular geometry.[14,15] We solve the resulting characteristic equation numerically using the implementation described in our previous work.[10]

The propagating modes obtained in this way can be classified as $EH_{l,p}$ and $HE_{l,p}$ modes (or the $TE_{0,p}$ and $TM_{0,p}$ modes for $l = 0$), according to the standard classification.[12] In this nomenclature, index l is the one specified by the trial functions of Eqs. (2) and (3), whereas index p is related to the radial order of the mode. In the self-imaging applications of annular-core fibers, however, it is useful to allow only the lowest-order radial mode ($p = 1$) to propagate, since only in such cases can clear self-images usually be observed.[4,5,8] This means that the self-imaging fibers typically have a thin core and a small refractive-index difference $n_1 - n_2$. The latter characteristic allows the vector modes of the fibers to be grouped into approximately linearly polarized $LP_{m,p}$ modes, some of which are illustrated in Fig. 1(b). The correspondence between the vector modes and the (scalar) $LP_{m,p}$ modes is such that the $LP_{0,p}$ mode corresponds to the $HE_{1,p}$ mode, the $LP_{1,p}$ mode corresponds to a superposition of the $HE_{2,p}$ mode, and the $TE_{0,p}$ or the $TM_{0,p}$ mode, and in general, the $LP_{m,p}$ mode ($m > 1$) corresponds to the superposition of the hybrid modes $EH_{m-1,p}$ and $HE_{m+1,p}$. In fact, Fig. 1(b) shows the squared modulus of the electric field of such a superposition, which is obtained by choosing $\phi = 0$ and real-valued constants for $C_1, \ldots, C_8$, yielding a y-polarized superposition field with a sinusoidal azimuthal modulation characteristic of the $LP_{m,1}$ modes [for $l = 0$ we obtain the $TE_{0,1}$ mode, as E_z then evidently equals zero in Eq. (2)].

Even though the propagation constants and the field profiles of the $LP_{m,1}$ modes could be conveniently obtained by use of the weakly guiding approximation, we are not going to describe the self-imaging phenomenon in terms of the $LP_{m,1}$ modes in this paper for two reasons. First, one cannot, in general, guarantee the accuracy of such an approximation when the trans-

verse geometry of the fiber is varied,[10] especially with the higher-order modes. Second, as the small difference between the propagation constants of the corresponding vector modes would then be completely neglected, one could not obtain any information on the beating effect that will occur when the vector modes propagate. For example, if the propagation constants of the vector modes $EH_{m-1,1}$ and $HE_{m+1,1}$ (the superposition of which corresponds to an $LP_{m,1}$ mode with $m > 1$) are denoted by β^- and β^+, respectively, one can associate with the propagation a beat length,

$$z_B = 2\pi/|\beta^- - \beta^+|, \tag{4}$$

in which the modes acquire a phase difference of 2π. Because of this effect, an $LP_{m,1}$ mode with $m > 0$ would lose, and later recover, its uniformly linear polarization state in a periodic fashion during propagation.

The propagation constants of the $LP_{m,1}$ modes do, however, possess one very useful property for our purposes. Namely, they approximately follow a quadratic dependence on index m in the form[5]

$$\beta = \beta_0 - \beta_1 m^2, \tag{5}$$

where β_0 and β_1 are positive constants. If the dependence given in Eq. (5) were strictly obeyed, the electric and magnetic fields at plane $z = 0$ would be perfectly imaged to the plane located at the Talbot distance given by

$$z_T = 2\pi/\beta_1, \tag{6}$$

with the phase factor of each mode being equal to $\exp(-i\beta_0 z_T)$. We will also use Eqs. (5) and (6) as a model for the self-imaging in our full-vectorial approach. This is accomplished by arranging the propagation constants of the vector modes according to index m of the corresponding $LP_{m,1}$ modes. Figure 2 shows two examples of the way the propagation constants place themselves in this model as a function of the square m^2. The dashed lines are least-squares fits to the data in the form of Eq. (5), from which an approximation to the Talbot distance z_T is obtained by use of Eq. (6). We will quantify the self-imaging capability of a certain fiber with the number obtained by multiplying the propagation distance z_T with the standard deviation σ of the fitted data. The product $s = \sigma z_T$ will then essentially characterize the standard deviation of the modal phases [in the propagation factors $\exp(-i\beta z)$] at the propagation distance $z = z_T$. The smaller the value of parameter s, the better are the self-imaging properties in general, i.e., with arbitrary excitation weights of the modes. Additionally, one must make sure that for each m the vector modes fulfill the condition $z_T \ll z_B$ so that the beating effect can be neglected.

3. Numerical Results

Here we present the results of our numerical calculations performed for fibers with four different values of core radius a. We fixed the value of the refractive-

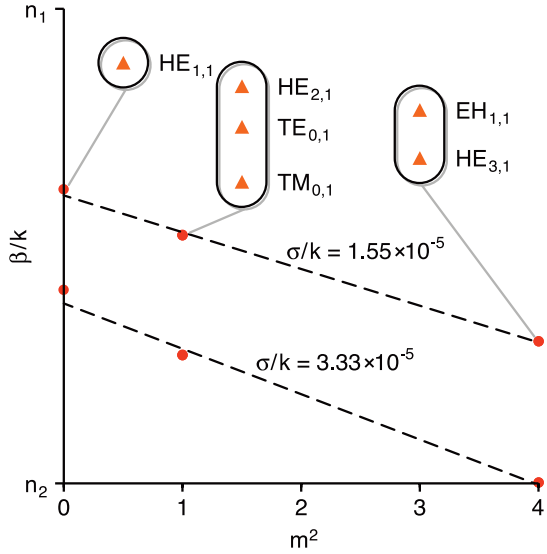

Fig. 2. (Color online) Normalized propagation constants β/k of the vector modes arranged according to index m of the $LP_{m,1}$ modes (dots). The insets illustrate that for $m > 1$ there are two modes (three modes for $m = 1$) with almost degenerate propagation constants (triangles). Dashed lines are least-squares fits with σ denoting their standard deviation. The core thickness is $d = 5.8\lambda$ (upper data) and $d = 3.5\lambda$ (lower data), and the other fiber parameters are $a = 5\lambda$, $n_1 = 1.457$, $n_2 = 1.455$, with λ denoting the vacuum wavelength.

index difference to be equal to $n_1 - n_2 = 0.002$, and chose the thickness of the core, $d = b - a$, to act as a variable parameter. Parameter d was varied from one fifth of a wavelength, $d = \lambda/5$, up to the value where the cutoff of the first mode with the radial index $p = 2$, i.e., the cutoff of the $HE_{1,2}$ mode, was encountered (near $d \approx 6.5\lambda$ for the chosen fibers). To obtain unambiguous results, we must require that at least two modes exist in the fiber even with the small values of d. Figure 3 shows the Talbot distances in the fibers obtained from Eqs. (5) and (6) using the least-squares fitting procedure. Also shown is the beat length z_B between the second-order modes $TE_{0,1}$ and $TM_{0,1}$, which turned out to be the smallest one among the modes of the chosen fibers. In Fig. 3, the Talbot distance z_T is seen to increase with the parameter a, but depend rather weakly on the core thickness, except for very thin fiber cores. There, a jump in the value of z_T can be seen whenever new modes ($EH_{m-1,1}$ and $HE_{m+1,1}$) are introduced as the core is made thicker. Qualitatively, the Talbot distances obey the dependence $z_T k \approx 16\pi^3 n_1 (a/\lambda)^2$, an expression that corresponds to the Talbot distance of a scalar field with a one-dimensional period equal to that of the circumference of the fiber ($\approx 2\pi a$), say in the x direction, in a dielectric material.[6,8] In addition, the condition $z_T \ll z_B$ is seen to be well fulfilled with the small fibers ($a \lesssim 15\lambda$), whereas with the large-diameter fibers, the distances z_T and z_B can be of the same order for $d \gtrsim 2\lambda$. This is important in cases where the self-imaging mostly relies on the second-order modes ($m = 1$ in terms of the $LP_{m,1}$ modes),

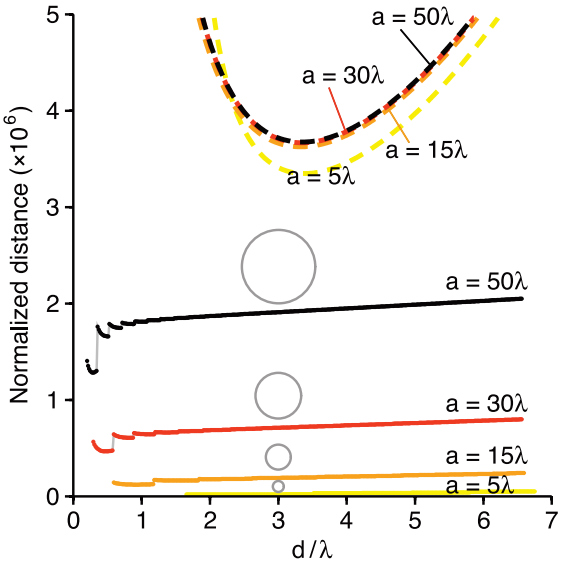

Fig. 3. (Color online) Normalized Talbot distance $z_T k$ (dots connected with gray curve) and the beat length $z_B k$ (dashed curve) of the modes $TE_{0,1}$ and $TM_{0,1}$ as a function of the normalized core thickness d/λ for four different values of the inner radius of core a. The relative sizes of the fiber cores are depicted by gray circles for $d/\lambda = 3$.

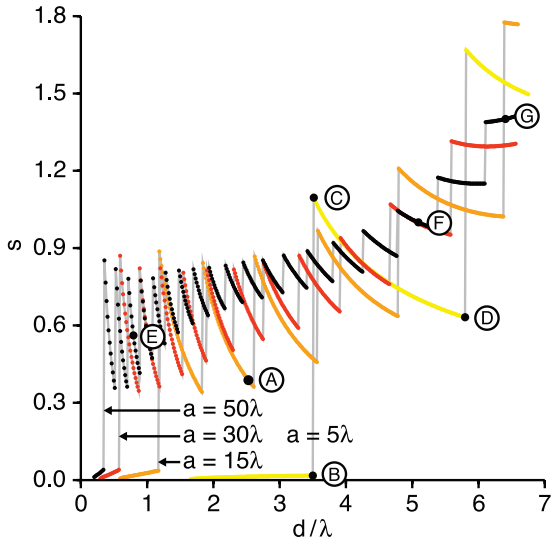

Fig. 4. (Color online) Parameter $s = \sigma z_T$ as a function of the normalized core thickness d/λ. The gray curves connect the data points corresponding to a certain value of the core radius a. The points labeled with the uppercase letters correspond to the cases of Fig. 5.

since the beating related to the numerous higher-order modes available in such large-diameter fibers will not be as significant within the first Talbot distance. However, if one wanted to create multiple self-images of the field at distances $z = z_T$, $2z_T$, $3z_T$, . . . , the beating of the higher-order modes would become relevant as well.

Another aspect, which is essential already at the first Talbot distance $z = z_T$, is the accuracy with which the propagation constants follow the quadratic dependence of Eq. (5). Figure 4 shows the behavior of the quantity $s = \sigma z_T$, which we choose to represent the accuracy. In this quantity, the jumps due to the new modes emerging as the core thickness is increased can be seen much more clearly than in the value of z_T alone in Fig. 3. The main contribution to the jumps thus comes from the standard deviation σ, which has a particularly large value when a propagation constant β is only slightly above the cutoff value $\beta = kn_2$. This can also be seen from the examples of Fig. 2, which correspond to the cases labeled C (lower data) and D (upper data) in Fig. 4. By averaging over the jumps in Fig. 4, one could say that parameter s, as a trend, increases with the thickness of the core. Furthermore, as the core radius a is made larger to increase the number of modes available in the imaging for a fixed value of d, the general self-imaging properties tend to deteriorate, i.e., the value of parameter s tends to grow. From Fig. 4, one can, in particular, note that the self-imaging works very well as long as the fiber supports only the two lowest-order $LP_{m,1}$ modes ($s \lesssim 0.05$), in which cases condition $z_T \ll z_B$ is also satisfied (see Fig. 3). Unfortunately, the self-imaging properties will not be nearly as good with any larger number of modes.

In Fig. 5, we give some examples of the self-imaging of the electric field from plane $z = 0$ to plane $z = z_T$ when the guided fiber modes are superposed with equal weights by making the value of the integral $\int\int |\mathbf{E}(r, \theta)|^2 r dr d\theta$ equal to unity for each mode. We chose $\phi = 0$ and real values for constants $C_1, \ldots, C_8$ in Eqs. (2) and (3), so that the individual modes could be grouped to form the approximate $LP_{m,1}$ modes at plane $z = 0$, as in Fig. 1(b). At plane

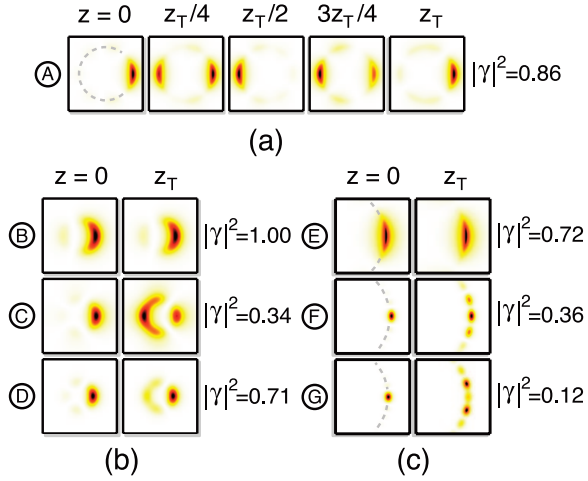

Fig. 5. (Color online) Intensity profiles of the fields in annular-core fibers at distances z shown above each column. The annular core is for clarity sketched with the gray dashed circle for $z = 0$ in (a) and (c), and the uppercase letters correspond to the points in Fig. 4. The squared modulus of the overlap integral, $|\gamma|^2$, between the fields at planes $z = 0$ and $z = z_T$ is shown at each row. The example plots are chosen to illustrate (a) some general features of the Talbot effect, (b) the deterioration of the self-image near modal cutoffs, and (c) the lowering of the image quality as the fiber core is made thicker.

$z = 0$, this superposition will result in a linearly polarized spot of light at the rim of the annular core. We evaluate the quality of the self-image of such a spot by calculating the overlap integral between the original field and its image as[8]

$$\gamma = N^{-1} \int\int \mathbf{F}^*(r,\ \theta,\ 0) \cdot \mathbf{F}(r,\ \theta,\ z_T) r dr d\theta, \quad (7)$$

where N is the number of guided modes in the superposition field denoted by $\mathbf{F}$, and the symbols $\cdot$ and $*$ denote the inner product and complex conjugation, respectively. With this particular superposition, Eq. (7) can be analytically simplified to the form $\gamma = N^{-1} \sum \exp(-i\beta z_T)$, where the summation is performed over propagation constants β of the modes. The closer the value of the squared modulus $|\gamma|^2$ is to unity, the better the self-image will be. Figure 5 shows the intensities of the fields calculated as $I(r, \theta, z) = |\mathbf{F}(r, \theta, z)|^2$.

Figure 5(a) first illustrates that some general features related to the free-space Talbot effect are also present in the annular fiber waveguide. The point corresponding to the parameters here is labeled with A in Fig. 4. Accordingly, at planes $z = z_T/4$ and $z = 3z_T/4$, the spatial frequency of the pattern is twice that of the original, whereas at plane $z = z_T/2$, an inverted image can be seen.[6,16] In Fig. 5(b), we illustrate how the introduction of a new $LP_{m,1}$ mode ($m = 2$ in this case) can reduce the quality of the self-image. The corresponding points of Fig. 4 are labeled B (below cutoff), C (just above cutoff), and D (far from cutoff). The squared modulus of the overlap integral $|\gamma|^2$ is seen to have a particularly small value when the mode is just above its cutoff. As a last illustration, in Fig. 5(c) we show that the quality of the self-image is reduced when the fiber core is made thicker, as suggested by the trend of parameter s in Fig. 4. The corresponding points of Fig. 4 are now denoted by E, F, and G. We note here that with the chosen superposition field, we could not obtain decent self-images at distances $z = 2z_T, 3z_t, 4z_T, \ldots$ (except when only two $LP_{m,1}$ modes were present) because of the large value of parameter s. Such images could, however, be obtained by allowing only a small portion of the fiber modes to propagate simultaneously, in which case the beating effect can limit the number of successive self-images.

4. Conclusions

We have used full-vectorial modal analysis to investigate the self-imaging properties of annular-core optical fibers. The self-imaging capability of a certain fiber was characterized by considering the standard deviation of the modal phases when the modes propagate a length equal to one Talbot distance. Within this approach, the general self-imaging properties could be characterized for an arbitrary superposition of the fiber modes.

Our results show that the vicinity of a modal cutoff deteriorates the self-imaging properties. As a trend, the self-imaging properties were also deteriorated when the number of fiber modes was made higher by increasing either the thickness or the inner radius of the fiber core. In addition, it turned out that the beating of the vector modes started to be significant when the radius of the fiber core exceeded the value of a few tens of optical wavelengths. Our results also confirm that, based on the analogy of considering the fiber as a wrapped-around slab waveguide, one can derive a rather good estimate for the Talbot distance, even with the smallest fibers.

M. Hautakorpi thanks the Jenny and Antti Wihuri fund and the Finnish Foundation of Technology for grants during the course of this work.

References

1. K. Patorski, "The self-imaging phenomenon and its applications," in *Progress in Optics,* E. Wolf, ed. (Elsevier, 1989), Vol. 27, pp. 1–108.
2. S. W. Allison and G. T. Gillies, "Observations of and applications for self-imaging in optical fibers," Appl. Opt. **33,** 1802–1805 (1994).
3. A. Mehta, W. Mohammed, and E. G. Johnson, "Multimode interference-based fiber-optic displacement sensor," IEEE Photon. Technol. Lett. **15,** 1129–1131 (2003).
4. C. Y. H. Tsao, D. N. Payne, and W. A. Gambling, "Modal characteristics of three-layered optical fiber waveguides: a modified approach," J. Opt. Soc. Am. A **6,** 555–563 (1989).
5. N. B. Baranova and B. Ya. Zel'dovich, "Talbot effect for whispering gallery modes and modes of tubular waveguides," in Technical Digest of the International Quantum Electronics Conference, IQEC'98 (1998), pp. 184–185.
6. T. Niemeier and R. Ulrich, "Self-imaging by ring-core fibers," in *Digest of Topical Meeting on Optical Fiber Communication,* I. D. Aggarwal, ed. (Optical Society of America, 1985), pp. 122–124.
7. A. Zoubir, C. Lopez, M. Richardson, and K. Richardson, "Femtosecond laser fabrication of tubular waveguides in poly(methyl methacrylate)," Opt. Lett. **29,** 1840–1842 (2004).
8. M. Wrage, P. Glas, D. Fischer, M. Leitner, N. N. Elkin, D. V. Vysotsky, A. P. Napartovich, and V. N. Troshchieva, "Phase-locking of a multicore fiber laser by wave propagation through an annular waveguide," Opt. Commun. **205,** 367–375 (2002).
9. A. P. Napartovich and D. V. Vysotsky, "Phase-locking of multicore fibre laser due to Talbot self-reproduction," J. Mod. Opt. **50,** 2715–2725 (2003).
10. M. Hautakorpi and M. Kaivola, "Modal analysis of *M*-type-dielectric-profile optical fibers in the weakly guiding approximation," J. Opt. Soc. Am. A **22,** 1163–1169 (2005).
11. J. D. Jackson, *Classical Electrodynamics,* 3rd ed. (Wiley, 1999).
12. A. W. Snyder and J. D. Love, *Optical Waveguide Theory,* 1st ed. (Chapman & Hall, 1983).
13. G. Keiser, *Optical Fiber Communications,* 3rd ed. (McGraw-Hill, 2000).
14. H. Ito, K. Sakaki, T. Nakata, W. Jhe, and M. Ohtsu, "Optical potential for atom guidance in a cylindrical-core hollow fiber," Opt. Commun. **115,** 57–64 (1995).
15. P. R. Chaudhuri, C. Lu, and W. Xiaoyan, "Scalar model and exact vectorial description for the design analysis of hollow optical fiber components," Opt. Commun. **228,** 285–293 (2003).
16. J. W. Goodman, *Introduction to Fourier Optics,* 2nd ed. (McGraw-Hill, 1996).